RESEARCH PAPER

Effect of Milling on Particle Shape and Surface Energy Heterogeneity of Needle-Shaped Crystals

Raimundo Ho • Majid Naderi • Jerry Y. Y. Heng • Daryl R. Williams • Frank Thielmann • Peter Bouza • Adam R. Keith • Greg Thiele • Daniel J. Burnett

ABSTRACT

Purpose Milling and micronization of particles are routinely employed in the pharmaceutical industry to obtain small particles with desired particle size characteristics. The aim of this study is to demonstrate that particle shape is an important factor affecting the fracture mechanism in milling.

Methods Needle-shaped crystals of the β polymorph of D-mannitol were prepared from recrystallization in water. A portion of the recrystallized materials was ball-milled. Unmilled and milled sieved fractions of recrystallized D-mannitol were analyzed by dynamic image analysis (DIA) and inverse gas chromatography (IGC) at finite concentration to explain the breakage/fracture behavior.

Results In the process of ball-milling, D-mannitol preferentially fractured along their shortest axis, exposing (011) plane with increased hydrophilicity and increased bounding rectangular aspect ratio. This is in contrary to attachment energy modeling which predicts a fracture mechanism across the (010) plane with increased hydrophobicity, and small change in particle shape.

Conclusions Crystal size, and more importantly, crystal shape and facet-specific mechanical properties, can dictate the fracture/cleavage behavior of organic crystalline materials. Thorough understanding of the crystal slip systems, combining attachment energy prediction with particle shape and surface characterization using DIA and IGC, are important in understanding fracture behavior of organic crystalline solids in milling and micronization.

INTRODUCTION

The stabilization of micrometer-sized drug particles with a high specific surface area and a narrow particle size distribution directly from solution crystallization is difficult at an industrial scale. Milling and micronization are still, at present, routinely used to obtain consistent particle size for downstream formulation processing. Reduction in particle size of the active pharmaceutical ingredient (API) is also sometimes necessary to improve the dissolution rate in gastrointestinal fluids (1), owing to the fact that 30–40% of new chemical entities (NCEs) display very poor water solubility (2). In the preparation of amorphous solid dispersions, dissolution behavior of the drug substance in the carrier is also aided by an increase in surface area (particle size reduction) (3).

Three dominant modes of stress application which can lead to comminution of particles include shear, impact and friction. Mechanical comminution processes involving high energy input such as jet milling, pin milling, high energy ball milling and high pressure homogenizers, as well as more

R. Ho (✉)
Global Pharmaceutical Research & Development, Abbott Laboratories
1401 Sheridan Road
North Chicago, Illinois 60064, USA
e-mail: raimundo.ho@abbott.com

M. Naderi
Surface Measurement Systems
5 Wharfside, Rosemont Road, Alperton
London HA0 4PE, UK

J. Y. Y. Heng · D. R. Williams
Surfaces & Particle Engineering Lab, Dept. of Chemical Engineering
Imperial College London
South Kensington Campus
London SW7 2AZ, UK

F. Thielmann
Novartis Pharma AG
Novartis Campus
4056 Basel, Switzerland

P. Bouza · A. R. Keith · G. Thiele
Micromeritics Analytical Services
4356 Communications Drive
Norcross, Georgia 30093, USA

D. J. Burnett
Surface Measurement Systems
2125 28th Street SW, Suite 1
Allentown, Pennsylvania 18103, USA

gentle processes such as comilling are well established techniques in the pharmaceutical industry. Although the desired particle size distribution can be economically and easily obtained from direct milling and micronization processes, the API may also undergo undesirable physical and/or chemical changes during the process, causing downstream processing, drug handling and storage issues. Solid-state transformations, crystal habit changes, mechanical hardening, and structural/chemical/thermodynamic stability are important subjects concerning material processability, end-product quality and functionality of micronized solid particles (4). As the particle size and crystal habit changes upon milling/micronization, the surface energetics of particles can also change (5). In most occasions, milled particles are notably more cohesive due to an increase in both surface area and surface energy, or they can have low bulk density due to their surface electrostatic charges, leading to issues in materials handling and powder flow.

Although particle size is traditionally considered as the major targeted result at the end of the milling or comminution, changes in the particle shape and surface properties are becoming increasingly recognized as a consequence of these processes as exemplified by the growing number of publications in this field. The particle shape is known to impact flowability (6) and compactability (7) of post-milled API, while the surface properties can affect wetting (8), aerosolization (9), mixing (10), compaction (11), and dissolution behavior (12).

Stress application in mechanical milling causes a reduction in particle size distribution by fracture of the crystals along specific crystallographic slip planes caused by dislocation movement as a consequence of plastic deformation. Gross crystal fracture occurs when the applied deformation energy reaches a level to overcome a critical dislocation density (13). During deformation, the most active slip planes are the source of defects and disorders. Common methods to identify slip planes in molecular crystals include attachment energy models, nano-indentation experiments, cleavage planes, and inferred data based on chemical bonding within the lattice.

In the milling of form I acetaminophen (paracetamol), the cleavage plane is an active slip plane with the lowest attachment energy, and it was shown, from IGC measurements, that this cleavage plane also has the lowest surface energy and is the most hydrophobic (14). Depending on the thermodynamic stability of the API, milling can lead to total/partial crystallinity loss, or generation of local amorphous domains (15,16). For crystals with different morphologies, the milling behavior can be drastically different. For instance, β-succinic acid crystals with plate-like morphology are more prone to crystallinity loss on milling compared to the needle-like morphology (17). The understanding of the relationship between milling/fracture behavior, the initial and resulting crystal shape and surface properties are, therefore, important in the design of milling processes, as well as other associated downstream processes for the milled products.

Crystals with needle-like morphology are known to be more difficult to process (18,19), but it is increasingly common to encounter particles of NCEs with elongated morphologies during discovery and early development. To this end, this study is primarily focused on the understanding of the fracture behavior of needle-shaped crystals by coupling advanced particle shape and surface energy characterization techniques using dynamic image analysis and inverse gas chromatography at finite concentration, respectively. This study is not intended to focus on the size reduction effect in milling, but to focus on the possible underlying mechanisms in the milling of needle-shaped particles. The subject of this investigation is a commonly used crystalline pharmaceutical excipient, the most thermodynamically stable β polymorph of D-mannitol.

DIA has become increasingly popular in the pharmaceutical industry as a means of extracting particle shape factors, in addition to particle size parameters, from digital images taken of small particles. As the particles are passed through the sensing zone, either by means of a liquid or dry gas dispersion mechanism, multiple 2-dimensional images of the particles are captured at high speed. These 2D digital images are processed in real-time with mathematical algorithms to obtain particle size parameters, such as the equivalent circular area diameter, as well as particle shape factors, such as aspect ratio, smoothness and circularity. This technique allows the simultaneous collection of particle size and shape information, without the need to predefine a particle shape profile for particulate systems under investigation.

IGC is a physicochemical characterization technique which can be used to measure the surface properties of powder materials, and recent advances in utilizing IGC at finite concentrations allow for the determination of surface energy distributions, which more accurately describe the anisotropic surface energy for materials. As crystalline materials are energetically anisotropic—different crystal planes can exhibit different chemistry, their surface energy may not be adequately described by a single average value (20). The anisotropic nature of D-mannitol and alpha lactose monohydrate, both widely used pharmaceutical excipients, have been studied in this way using IGC (5,21). This technique is used, for the first time in this study, to determine the impact of milling on the surface energy distributions of multi-faceted organic pharmaceutical crystals.

MATERIALS AND METHODS

Recrystallization

To ensure that the starting material has a needle-shaped morphology, a saturated solution of D-mannitol (Ph Eur

Pearlitol 160C, Roquette, France) in deionized water at 50°C was allowed to cool at room temperature (~25°C). The recrystallized solids were filtered and dried in an oven at 70°C over 24 h.

Ball-milling

Half of the recrystallized D-mannitol powder (~500 g) was milled with a porcelain ball-mill (Pascall Engineering, Suffolk, U.K.) with 20 ceramic balls, 1.5 mm in diameter, for 4 h. The resultant milled powders were then sieved using a series of test sieves to obtain the following fractions: 63–125 μm, 125–180 μm, 180–250 μm and 250–355 μm. The unmilled powders were also subjected to the same sieving procedure to yield the same sieve particle size fractions. The sieved materials were rested at room conditions (23°C, 40% RH) for at least 5 days prior to further experiments.

Specific Surface Area Analysis

The BET specific surface area of individual sieve fractions was determined from nitrogen adsorption isotherms at 77 K using a surface area analyzer (Tristar 3020, Micromeritics, Norcross, GA). The samples were degassed under vacuum for 16 h at 25°C prior to nitrogen adsorption.

Particle Shape Analysis

Particle shape information was obtained by dynamic image analysis (Particle Insight, Model P01/00000/00, Micromeritics/Particulate Systems, Norcross, GA). This DIA system has a recommended measuring range between 3 and 300 μm, but can measure particles up to 600 μm. Isopropanol (HPLC grade, Sigma-Aldrich, Poole, U.K.) was used as dispersant. Approximately 100 to 500 mg of sample from the well-mixed bottle was transferred to the sample chamber (with a total liquid volume of approximately 30 ml) of the instrument for particle shape analysis. The instrument utilizes a recirculating fluidic path which randomizes particle orientation as they are passed through the detection area of the instrument. This operation also ensures that over time, a full homogeneous sampling is achieved from the sample as particles are re-analyzed during recirculation. Prior to particle shape measurements, the liquid dispersion conditions, measurement duration, and dark pixel concentration were optimized to achieve a standard deviation between measurements of less than 3%. The optimized pump speed was at 17% of full power, and measurement duration was 500 s for each sample. Each measurement contained at least 50,000 in-focus particle counts to ensure representative sampling.

Surface Energy Distribution Analysis

The dispersive surface energy distributions of the milled sieve fractions were measured by the iGC-Surface Energy Analyzer instrument (IGC-SEA, Surface Measurement Systems, London, U.K.) equipped with a flame ionization detector. Each sieve fraction of D-mannitol was packed into separate standard pre-silanized columns (300 mm length × 4 mm ID) with silanized glass wool sealed at each end to prevent sample movement during the experiment. Columns were filled with approximately 1 g of material and then conditioned *in-situ* in the IGC-SEA with helium for 2 h at 30°C to remove physisorbed water. The IGC-SEA has a unique injection mechanism which allows the precise control of the injection size, thereby precise amount (n, *mole*) of probe vapor can be passed through the sample column to achieve a specific probe surface coverage, n/n_m (where n_m is the probe monolayer coverage). If a series of probe vapors is injected over a range of surface coverages, a surface free energy profile can be mapped, resulting in a profile of surface energy as a function of coverage. A series of purely dispersive n-alkane vapor probes (decane, nonane, octane, heptane) (HPLC grade, Sigma-Aldrich, Poole, U.K.) were used as probe molecules, and methane was used for dead volume determination. Helium, at a flow rate of 10 sccm (standard cubic centimeter per minute), was used as carrier gas for all injections. Dispersive surface energy profiles and distributions were calculated directly using Cirrus Plus software (version 1.1.0, Surface Measurement Systems, London, U.K.) following the Dorris-Gray approach. The reported surface energy profiles and distributions are the average of two identical runs of probe injections on each sample column, and the standard deviation of γ^d data measured in this study is no more than 3% at any probe surface coverage.

Scanning Electron Microscopy (SEM)

SEM images were acquired with a Jeol scanning electron microscope system (JSM-6390, Jeol, Tokyo, Japan), at a working distance of 14 mm and an accelerated voltage of 15 kV. Particles were gold-coated in argon using a sputter coater (Desk IV, Denton Vacuum, Moorestown, NJ) at a current of 40 mA for 2 min prior to SEM imaging.

RESULTS AND DISCUSSION

Crystal Habit, Surface Chemistry and Theoretical Fracture Behavior of D-mannitol

Kaminsky *et al.* reported that D-mannitol exhibits the crystal planes (011), (010), (120), (110), and (210) (22). The

dispersive, γ^d, polar, γ^p, and total, γ^T, surface energies of plane (011), (120) and (010) have been reported previously (23). The (010) plane has the lowest surface energy, and is the most hydrophobic crystal plane, whilst the (011) has the highest surface energy, and is the most hydrophilic in nature due to the high concentration of hydroxyl functional groups on this crystal plane (23).

When particles are subjected to mechanical fracture as a result of particle-particle, particle-ball and particle-wall collisions upon ball-milling, it is postulated that the particles will preferentially break up in two dominant ways, depending on the shape of the particles: 1) particles fracturing along their shortest dimension amongst all orientations, or 2) the exposure of an active crystal slip plane with a low predicted attachment energy. Attachment energy calculation is one of the common techniques used to identify slip planes in molecular crystals. Based on growth morphology model (24), attachment energy is the energy released on the attachment of a growth slice or a new layer of molecules to a growing crystal surface. As the most probable growth layer on a given face is the one bound most easily to the crystal face, such layer could be obtained by cleaving the crystal parallel to that face. Although attachment energy data, on their own, may not always explain crystal fracture behavior (25) as crystal displaying strong mechanical anisotropy can have multiple slip systems, attachment energy data are still useful starting point to understand the potential change in particle shape before actual milling runs are conducted. Crystal planes with low attachment energies are usually slip planes of the highest molecule density with largest d-spacing amongst all planes in the crystal. By means of dislocation propagation, the slip planes are more energetically favorable to slip along a certain direction within the crystal structure system (the slip system). Under this mode of mechanical fracture, a change in surface properties toward the crystal plane corresponding to that of a low attachment energy plane is expected. An example of this mode of fracture is demonstrated by the milling of acetaminophen in an earlier study (14), in which the dispersive surface energy was found to increase from 34.0 to 41.0 mJ/m^2, reflecting an increase in the contribution of exposed crystal plane (010) (the slip plane with the lowest predicted attachment energy).

Nevertheless, the assumption that particle breakage is dominated by a low attachment energy crystal plane may only be valid when the attachment energy corresponding to that plane in consideration is far lower than those attachment energies corresponding to all other possible crystal slip systems. It may also hold true when the crystal is not experiencing a biased force loading on specific crystal planes during impact or shear deformation upon milling, and also surface flaws are not providing favorable initiating points for crack propagation to occur. Furthermore, at the molecular scale, lattice planes which contain zig-zag, or corrugated molecular layers will have significant energy barrier for slip occurrence, even if the attachment energy is low (25).

In the case of needle-shaped D-mannitol, the two weakest attachment energy planes are predicted to be (010) and (110) (26), which are both parallel to the c-axis of the crystal lattice and the growth direction of the crystal (Fig. 1). In reality, the force experienced by particles with a low aspect ratio, defined as ratio of the minimum Feret diameter to maximum Feret diameter, can be more easily transferred along a short distance via stress transfer, as the impact force can be readily dissipated by fracture of the plane along a short dimension. It is clear, from Fig. 1, that the fracture of D-mannitol based on either geometry (Fig. 1a), or thermodynamics from energetic consideration (Fig. 1b) will result in substantial differences in the particle shape and surface energy of the final milled products. The fracture mechanism based on geometry will create D-mannitol particles with high aspect ratio, and increased hydrophilicity (as a consequence of the exposure of plane (011)), whereas the fracture mechanism based on thermodynamics will create particles with similar aspect ratio as the original premill crystals, but with an increased hydrophobicity (as a consequence of the exposure of plane (010)). To illustrate and understand how D-mannitol with a needle morphology would break up upon milling, an assessment is performed, in this study, based on the particle shape and surface energetic distributions of the unmilled and milled materials in various sieve fractions.

Surface Areas and Crystal Shape Distributions of Unmilled and Milled D-mannitol

To qualitatively understand the quality of the recrystallized D-mannitol and the sieving performance, BET specific surface areas of the unmilled and milled fractions of D-mannitol were obtained by standard nitrogen adsorption technique (Fig. 2). As expected, milled D-mannitol in all sieve fractions have consistently larger BET specific surface areas compared to unmilled D-mannitol. An increase in the specific surface area for the milled samples, as the sieve size is reduced, revealed that the milled samples are predominantly single primary crystals, and that sieving was able to provide adequate particle size classification of the recrystallized material. However, the 250–355 µm sieve fraction of the unmilled material did not follow the same increasing trend in specific surface area as particle size is reduced. The reason could be attributed to a small number of agglomerated primary particles in this fraction, thus leading to a higher than expected specific surface area value. These porous agglomerates of primary particles in this fraction are identifiable by SEM (Fig. 3). Apart from the unmilled sieve fraction of 250–355 µm, each fraction appeared to contain primarily unagglomerated crystals. A
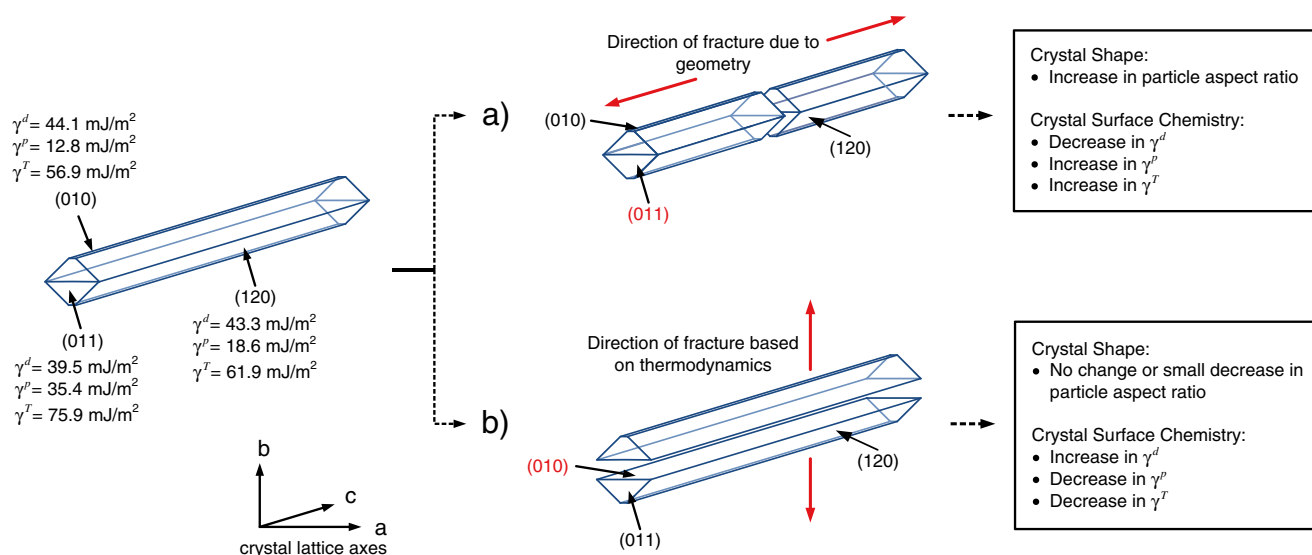
Fig. 1 Scenarios representing the fracture of D-mannitol with a needle morphology: (**a**) fracture direction across (011) and (**b**) fracture direction across (010). Surface energy components of facet (010), (011) and (120) for D-mannitol were taken from Ho et al. (23).

clear distinction can be made between the milled and un-milled fractions.

In DIA, the particle size is usually described based on the diameter of the circle with the same projected area expressed in their volume/mass ratio. However, needle particles cannot be accurately described by its spherical diameter. As sieving would primarily classify particles based on the shortest dimension of the needles, the bounding rectangular (BR) width, which is defined as the shorter dimension of the smallest encasing rectangle of the projected area (Fig. 4), would provide a much accurate particle size descriptor for sieved powders with needle-like morphology.

The number-based mean BR aspect ratio, which is the ratio of the shorter to longer dimension of the smallest encasing rectangle of the projected area, is plotted as a function of the average BR width of the sieve fractions in
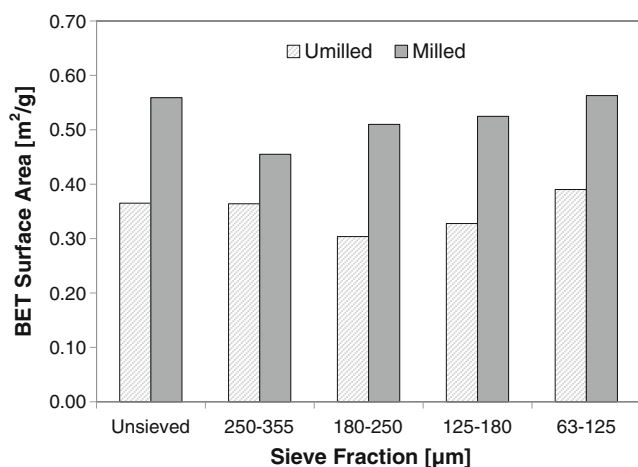

Fig. 2 BET specific surface areas of all unmilled and milled sieved fractions of D-mannitol.

Fig. 5. (It should be noted that the bounding rectangular aspect ratio is defined in this study as the ratio of BR width to BR length, to be consistent with new standardized definition of aspect ratio. The BR aspect ratio is defined as the ratio of BR length to BR width by the DIA instrument, Particle Insight, and this definition was not used in this work. The instrument was automatically set at a resolution of 1.3 µm per pixel in order to provide adequate sensitivity of the smaller particles in the milled fractions.)

The four sieve fractions together with the two pre-sieved samples of milled and unmilled D-mannitol show clear differences in their BR aspect ratios. Comparing between milled and unmilled D-mannitol at the identical BR width, it is clear that the milled materials exhibit consistently larger BR aspect ratios, implying that milled D-mannitol needles are shorter in length than unmilled D-mannitol. The milled samples have, on average, 7.7% larger BR aspect ratio compared to the original unmilled samples. The results by DIA provide clear evidence of the geometric fracture mechanism as shown in Fig. 1a. Although D-mannitol crystals have fractured along the (011) plane upon milling, further analysis of the particle shape data also revealed that the particles have also fractured in parallel to the c-axis of the crystal structure, based on the variation of the BR widths for the milled and unmilled materials. The range of the BR width for unmilled D-mannitol varies between 19 µm and 28 µm, whereas for the milled D-mannitol, the range varies between 17 µm and 24 µm. The smaller overall BR width for the milled samples is indicative of particle fracture across planes in parallel to the c-axis of the needle, with (010) or (110) being most likely, due to their low attachment energies from molecular modeling (26).

Particle shape, similar to particle size, can be represented based on number, surface area and volume. Volume-based

Fig. 3 SEM micrographs of different sieve fractions of unmilled and milled D-mannitol.
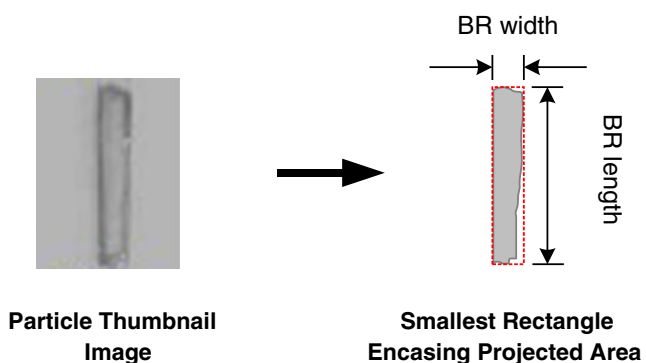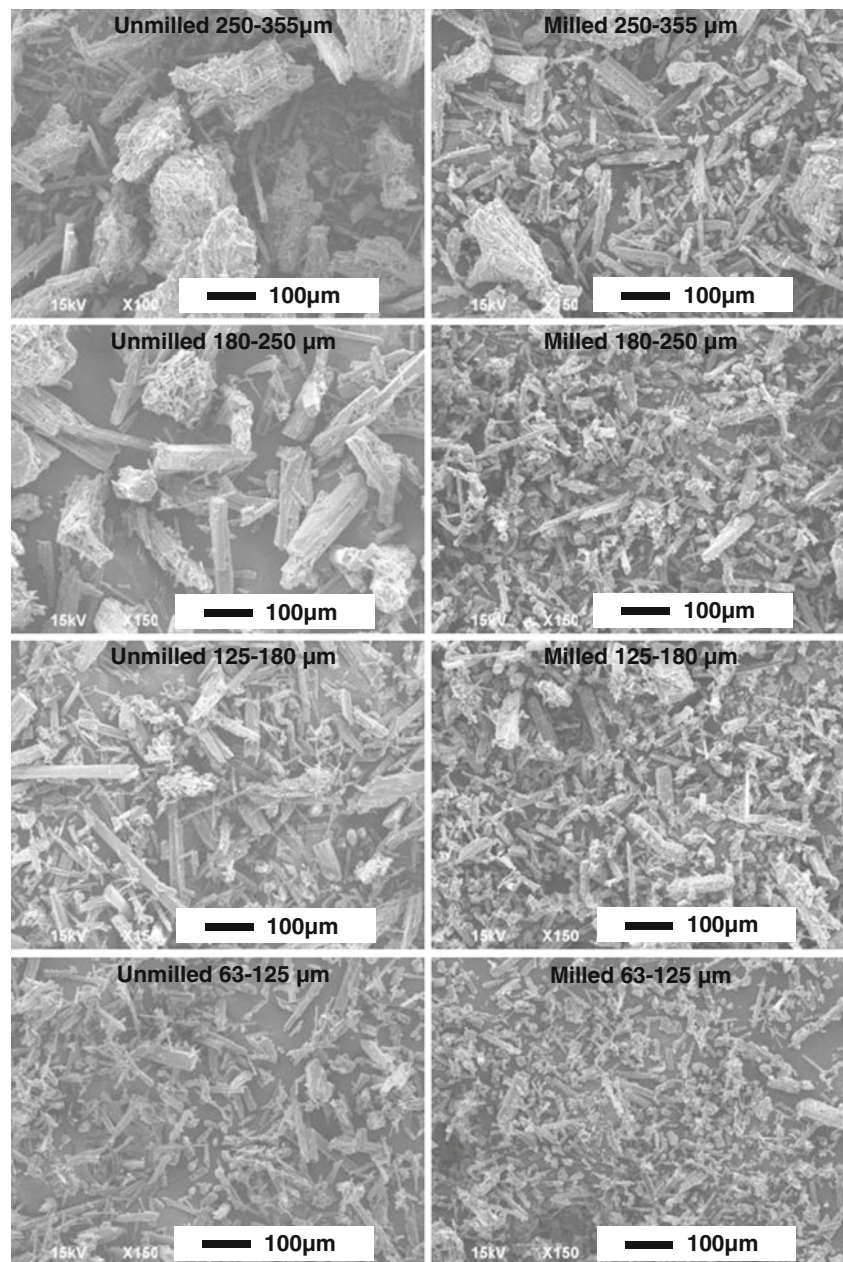

Fig. 4 Definition of bounding reactangular width and length. The bounding rectangular aspect ratio is defined as the width to length ratio.

methods are sensitive to the large particles in a sample due to their large volume, whereas number-based methods are sensitive to the small particles in a sample as they are typically present in large numbers. Since DIA is a number-based technique (a direct measurement of 'each' particle image), the true result is number-weighted. However, surface-area and volume-based particle shape distributions can be estimated from the number data, assuming a thickness in the third dimension equal to the average of the two other dimensions. With this approach, a particle with a particular shape will have an associated surface area and volume, thus the surface area % and volume % distribution can be computed. From the SEM images on Fig. 3, the milled sieve fractions contain a small portion of smaller fragmented particles as a consequent
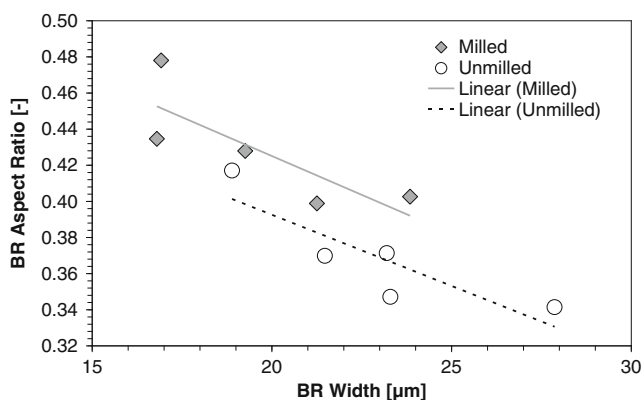
Fig. 5 Bounding rectangular aspect ratio (number-based) as a function of bounding rectangular width (number-based) for milled and unmilled D-mannitol.

of milling. To illustrate their shape and effects to the milled data, the volume-based and number-based BR aspect ratio cumulative percentiles for the pre-sieved unmilled and milled D-mannitol are presented in Table I. Number-based percentiles, which are sensitive to these smaller particles, are consistently higher than volume-based percentiles for both milled and unmilled materials, revealing that the smaller particles are essentially shorter in length (larger BR aspect ratio) than the bigger particles (smaller BR aspect ratio). The larger BR aspect ratios measured for these smaller particles are consistent with SEM images. However, using either number-based or volume-based distributions, the change in BR aspect ratio upon milling is identical—an increase in BR aspect ratio can be seen in all cases.

An understanding into which particular particle size ranges may be more susceptible to breakage in this system can be obtained by investigating the difference between initial and resulting aspect ratio of different sieved particles before and after milling. It should be noted that milling not only induces shape changes, but also particle size changes. However, needle-shaped particles are primarily classified in sieving based on their shortest dimensions, which are not expected to change significantly upon milling as revealed by the particle BR width in Fig. 5. Therefore, it is a valid to

assume that pre- and post-milled sieve fractions can be compared directly to deduce the size effect on shape changes. Figure 6 shows that the percentage change in BR aspect ratio for different sieve fractions of D-mannitol after milling. The positive values correspond to an increase in aspect ratio from particles of all sizes upon milling. With the exception of the biggest sieve fraction (250–355 μm), the largest increase in BR aspect ratio can be seen in the 180–250 μm particle size range with 28.6% increase. As the particle size decreases, this positive change in aspect ratio is less. The large increase in BR aspect ratio for 180–250 μm particle size range implies that particle breakages are dominated by the geometric cleavage mechanism across the (011) plane. For larger particles (i.e. longer needles), one would also expect to have a higher occurrence of breakages, compared to smaller particles (i.e. shorter needles), whereby the probability of breakages across the (011) plane would be less. It is postulated that a critical particle size and aspect ratio may be reached by further milling, such that the dominant fracture mechanism is reversed to one that is thermodynamically favored as depicted in Fig. 1b. The small percentage change in BR aspect ratio for the 250–355 μm sieve size particles can be explained by the agglomerated particles in this sample. If the agglomerates were separated into the primary needle particles in milling, this effect would most probably be associated with a decrease in particle BR aspect ratio. Therefore, it is not surprising that the small BR aspect ratio increase for this size range may have been influenced by such effects, as this fraction contains a proportion of agglomerated particles.

Relationship Between Surface Energy Distributions and Crystal Shape

The dispersive surface energy profiles of milled D-mannitol measured by the IGC-SEA are displayed in Fig. 7. The γ^d profile is a map of dispersive surface energies at different

Table I Comulative Percentiles of Number-Based and Volume-Based Bounding Rectangular Aspect Ratios for Unsieved Milled and Unmilled D-mannitol

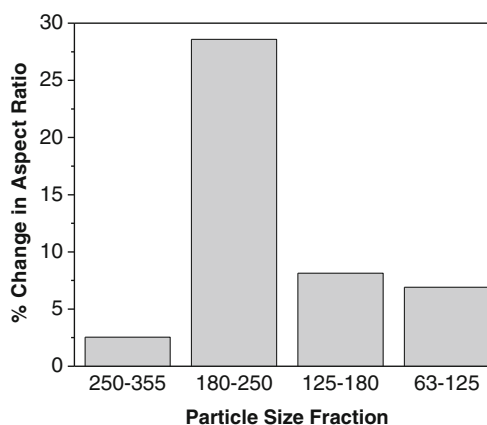| Percentiles	Unmilled (Unsieved)		Milled (Unsieved)	
	Number	Volume	Number	Volume
10%	0.87	0.76	0.93	0.86
25%	0.66	0.54	0.84	0.59
50%	0.45	0.36	0.61	0.46
75%	0.30	0.25	0.39	0.29
90%	0.21	0.18	0.27	0.21

Fig. 6 Percentage change in bounding rectangular aspect ratio (number-based) for different sieved particles upon milling.
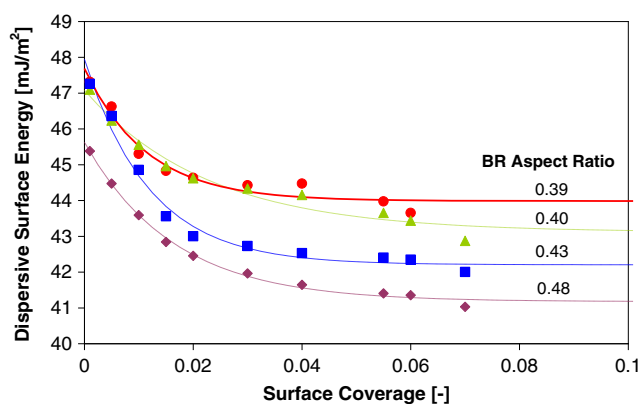
Fig. 7 Dispersive surface energy profiles of milled D-mannitol sieve fractions as a function of bounding rectangular aspect ratios (number-based mean).

probe surface coverages, i.e. isosteres. Real materials display surface structural and chemical heterogeneity, which in turn, give rise to their surface energetic heterogeneity. For a multi-faceted crystal with perfectly smooth surfaces, the energetic heterogeneity is attributed to the exposed surface functional groups at each crystal plane. When the crystallization is conducted in a slow and well-controlled process, structural heterogeneity, such as crystal imperfections, surface irregularities, surface pores, dislocation sites, crystal growth steps, as well as chemical heterogeneity, such as surface contaminants, chemical degradants, surface domains of thermodynamically unstable solid forms, will only have negligible impact on the surface energetic heterogeneity of materials.

The determination of a γ^d profile of a material by IGC-SEA is based on the formation of a physisorbed molecular layer of alkane probe molecules on the surface of the sample. Depending on the molecular cross-sectional area of the probes, different amount of alkane molecules are injected into the IGC sample column to achieve a particular probe surface coverage, thereby allowing the determination of γ^d at a predefined isostere. In measuring the γ^d profile, the surface energy heterogeneity of the sample can be determined. If the surface energy profile is integrated across the entire range of surface coverages (0–100%) (referred to as 'area under curve' method), a surface energy distribution is also obtained, analogous in principle to a particle size distribution, wherein particle size is replaced by surface energy and frequency density is replaced by area increment or surface area percentage. To enable an integration across the full surface coverage range, the experimental datapoints were extrapolated with an exponential decay function in the form of $y = y_0 + Ae^{-x/t}$, where y_0 is the offset, A is the amplitude and t is the decay constant. In the authors' experience, this exponential function provides the most consistent fit of data from IGC heterogeneity experiments for organic crystalline materials. The regression coefficient, R^2, for the linearity of

fit of the retention data to the Dorris-Gray γ^d analysis was proposed as a criterion for predicting the robustness of γ^d profiles obtained (26). In this work, γ^d values determined from the alkane line with a R^2 coefficient better than 0.9995 were used. Although this is lower than the recommended R^2 value of 0.9999 for low surface area materials, the reproducibility (standard deviation) of γ^d profiles is less than 3% in this work.

The surface energy distributions for the milled D-mannitol fractions are shown in Fig. 8. The γ^d distribution is a clear representation of the absolute range of the energy heterogeneity, and allows for computation of the geometric mean γ^d value. Common IGC experiments at infinite dilution skew γ^d values toward the most active surface sites, thus preventing the unambiguous delineation of chemically indifferent, yet structurally different materials exhibiting active sites of similar adsorption free energies. A schematic comparison between IGC at traditional infinite dilution and at finite concentration range is displayed in Fig. 9. At finite concentration, the utility of an increasing concentration of probe molecules leads to the access of low energy sites, therefore the entire surface can be characterized. The surface energy distribution is not dependent on the total surface area of the sample, as the availability of energy sites is expressed as percentages, but is dependent on the contribution of different energy sites to the overall distribution. IGC at finite concentration, therefore, can offer much detailed energetic profile of the surface than traditional IGC experiments at infinite dilution.

From Figs. 7 and 8, it is clear that the dispersive surface energies are related to the crystal shape of milled D-mannitol. As the BR aspect ratio increases, the dispersive surface energy profiles display a downward trend toward lower dispersive surface energy. The mean γ^d values, as measured from the distributions of surface energy depicted in Fig. 8, decreases from 44.7 to 42.1 mJ/m² (6% difference) as the BR aspect ratio increases from 0.39 to 0.48. This
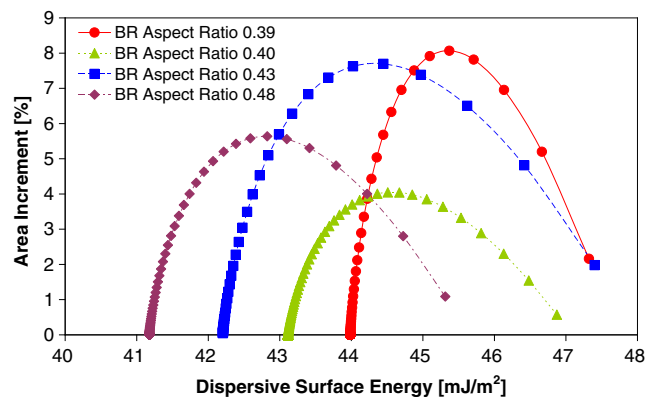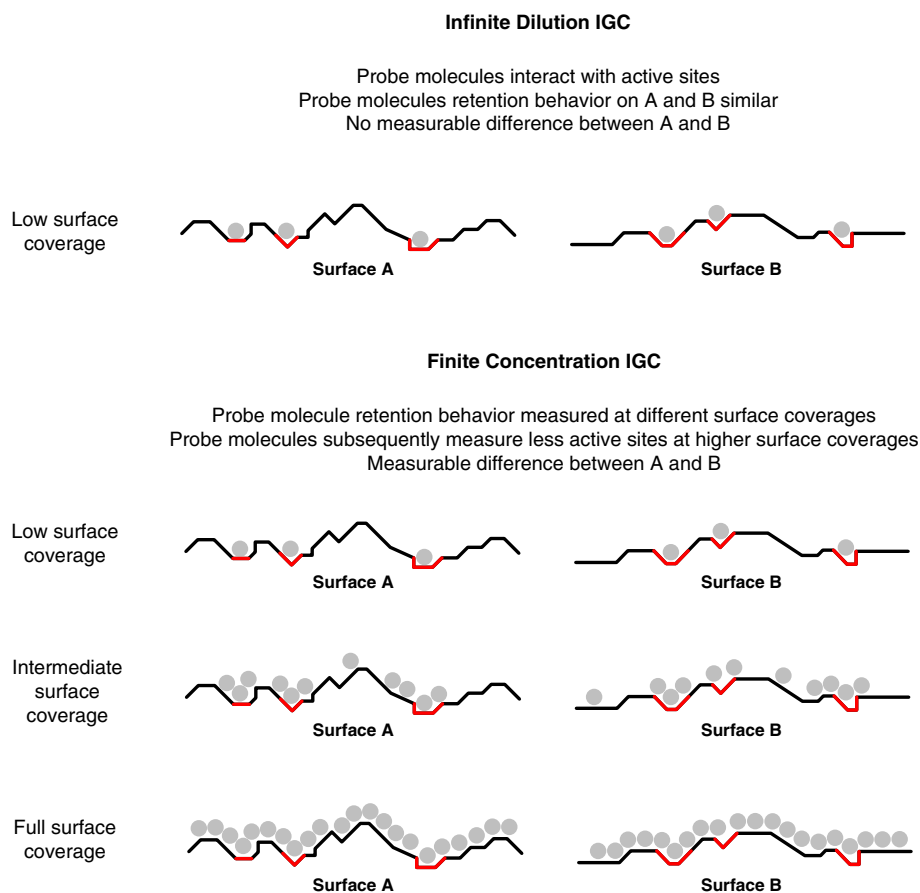

Fig. 8 Dispersive surface energy distributions, obtained by 'area under curve' method, for milled D-mannitol sieve fractions with different bounding rectangular aspect ratios (number-based mean).

Fig. 9 Schematic of IGC measurements at infinite dilution and finite concentration for two structurally different surfaces.

Infinite Dilution IGC

Probe molecules interact with active sites
Probe molecules retention behavior on A and B similar
No measurable difference between A and B

Low surface coverage

Surface A **Surface B**

Finite Concentration IGC

Probe molecule retention behavior measured at different surface coverages
Probe molecules subsequently measure less active sites at higher surface coverages
Measurable difference between A and B

Low surface coverage

Surface A **Surface B**

Intermediate surface coverage

Surface A **Surface B**

Full surface coverage

Surface A **Surface B**

reduction of dispersive surface energy can be explained by the exposure of crystal plane (011) of D-mannitol needles upon milling. Albeit just a small reduction in the mean γ^d, this is rather significant due to the fact that the absolute γ^d difference between (010) and (011) is less than 5 mJ/m^2 (Fig. 1), and that the standard deviation for experimental SEA γ^d data is less than 3% in this work. From the increase in BR aspect ratio, it would be expected that the contribution of (011) plane would increase. The (011) plane, which has the lowest dispersive surface energy (39.5 mJ/m^2), would therefore start to dominate the overall surface chemistry as D-mannitol is milled. The creation of new (011) surface in milling leads to an increase in the total surface area, but the (011) contribution to the overall surface energy distribution also increases, leading to a decrease in the mean γ^d. As this crystal plane is intrinsically more hydrophilic, milling would therefore increase the overall hydrophilicity of the material. The increase in hydrophilicity of D-mannitol upon milling has direct implications in process such as wet granulation, whereby one would expect the wettability of D-mannitol by the liquid binder to increase. Since the (011) plane also has higher total surface energy, the cohesivity of D-mannitol is expected to increase by milling. It is interesting to note that the change in surface polarity upon milling of D-mannitol is in direct contrast to

the milling of acetaminophen reported in an earlier work (14), in which the γ^d would increase as a result of the exposure of (010) crystal plane, leading to an increase in the overall surface hydrophobicity.

The glass transition temperature of D-mannitol is reported to be 10.7°C ($T_{g, onset}$) (27), and even for totally amorphous D-mannitol, the amorphous state can be recrystallized quickly at room temperature (28). Therefore, although milling may induce amorphous domains on the surface of D-mannitol, the milled samples used in this study were rested for sufficient period of time to ensure that the differences in surface energy distributions are not attributed to minor surface amorphous domains. Minor dislocations and polymorphic conversion from the stable β polymorph to the metastable α polymorph are possible in milling of D-mannitol (29), but the generation of active sites by means of dislocations or a metastable phase would typically be accompanied by an increase in surface energies due to their higher free energy. As such increase in surface energy was not observed, any changes in the surface properties of milled D-mannitol would, therefore, not be attributed to such effects in this study.

The two fracture mechanisms described in this study (as depicted in Fig. 1) are not expected to be the only possible mechanisms for fracture, as particles under impact loading

conditions will also suffer from attrition due to chipping in addition to fragmentation of the needles across the (011) plane (30), but the results here have shown that the mechanism in this type of rotary ball-milling process is dominated by fragmentation of the needles across the crystal plane with a small external area (i.e. the shortest dimension). As ball milling is dominated by impact breakages (interparticle, ball-particle, and particle-wall), it is expected that similar breakage mechanism would occur in other mill types as determined also by impact breakages at similar stress conditions and impact velocities. The geometric and thermodynamic fracture mechanisms are also not expected to be mutually exclusive, but at the bulk level, the geometric mechanism is the statistically dominating mechanism for needle-shaped particles and size range of particles under study in this work.

Our results show that the crystal shape can affect the fracture/cleavage behavior of organic crystalline materials. The surface properties of the resulting milled particles are closely related to the underlying fracture behavior. For crystals with a needle-like morphology, the particles may be more susceptible to breakage along their short axes, despite the fact that they are not the most active slip planes, as demonstrated in the example of D-mannitol with a low attachment energy plane of (010). When such instance occurs, the attachment energy model will fail to predict correctly the milling behavior of materials. From a particle engineering perspective, a careful and thorough understanding of the crystallographic structure of the material and the associated slip systems, combining particle shape and surface characterization tools such as DIA and IGC, are crucial in understanding fracture behavior of crystalline materials in pharmaceutical process R&D.

CONCLUSION

Milling and micronization of particles are routinely employed in the pharmaceutical industry as a convenient and cost-effective way to obtain particles with desired particle size characteristics for handling, processing, and formulation development. The prediction of milling behavior and performance requires a thorough knowledge of the particle size, the various slip systems comprising the particle shape, as well as the anisotropic mechanical properties of the crystal. In the example of needles, the fracture behavior may be more dominated by the impact mechanism and the geometry of the particles rather than the internal molecular interactions within the crystal lattice. This study shows that utilizing attachment energy prediction, combining with particle shape and surface energetic characterization tools are necessary to thoroughly explain the underlying fracture behavior of crystalline solids.

As demonstrated in this study, the surface properties are directly dictated by the mechanism of milling, leading to substantial change in the surface chemistry—increase or reduction in surface polarity are both equally viable. It is expected that if the direction of stress deformation can be controlled in milling, particle shape and surface properties may be feasibly engineered to tailor for downstream processing and formulation requirements.

REFERENCES

1. Rasenack N, Müller BW. Dissolution rate enhancement by *in situ* micronization of poorly water-soluble drugs. Pharm Res. 2002;19 (12):1894–900.
2. Lipinski C. Poor aqueous solubility: an industry wide problem in drug discovery. Am Pharm Rev. 2002;5:82–5.
3. Alonzo DE, Gao Y, Zhou D, Mo H, Zhang GGZ, Taylor LS. Dissolution and precipitation behavior of amorphous solid dispersions. J Pharm Sci. 2011;100(8):3316–31.
4. Chow AHL, Tong HHY, Chattopadhyay P, Shekunov BY. Particle engineering for pulmonary drug delivery. Pharm Res. 2007;24 (3):411–37.
5. Ho R, Wilson DA, Heng JYY. Crystal habits and the variation in surface energy heterogeneity. Cryst Growth Des. 2009;9(11):4907–11.
6. Feeley JC, York P, Sumby BS, Dicks H. Determination of surface properties and flow characteristics of salbutamol sulphate, before and after micronisation. Int J Pharm. 1998;172(1–2):89–96.
7. Rasenack N, Muller BW. Crystal habit and tableting behaviour. Int J Pharm. 2002;244(1–2):45–57.
8. Ho R, Dilworth SE, Williams DR, Heng JYY. Role of surface chemistry and energetics in high shear wet granulation. Ind Eng Chem Res. 2011;50(16):9642–9.
9. Traini D, Rogueda P, Young P, Price R. Surface energy and interparticle forces correlations in model pMDI formulations. Pharm Res. 2005;22(5):816–25.
10. Mackin L, Sartnurak S, Thomas I, Moore S. The impact of low levels of amorphous material (<5%) on the blending characteristics of a direct compression formulation. Int J Pharm. 2002;231 (2):213–26.
11. Fichtner F, Mahlin D, Welch K, Gaisford S, Alderborn G. Effect of surface energy on powder compactibility. Pharm Res. 2008;25 (12):2750–9.
12. Danesh A, Connell SD, Davies MC, Roberts CJ, Tendler SJB, Williams PM, *et al.* An *in situ* dissolution study of aspirin crystal planes (100) and (001) by atomic force microscopy. Pharm Res. 2001;18(3):299–303.
13. Olusanmi D, Roberts KJ, Ghadiri M, Ding Y. The breakage behaviour of Aspirin under quasi-static indentation and single particle impact loading: Effect of crystallographic anisotropy. Int J Pharm. 2011;411(1–2):49–63.
14. Heng JYY, Thielmann F, Williams DR. The effects of milling on the surface properties of form I paracetamol crystals. Pharm Res. 2006;23(8):1918–27.
15. Ward GH, Schultz RK. Process-induced crystallinity changes in albuterol sulfate and its effect on powder physical stability. Pharm Res. 1995;12(5):773–9.
16. Descamps M, Willart JF, Dudognon E, Caron V. Transformation of pharmaceutical compounds upon milling and comilling: The role of Tg. J Pharm Sci. 2007;96(5):1398–407.
17. Chikhalia V, Forbes RT, Storey RA, Ticehurst M. The effect of crystal morphology and mill type on milling induced crystal disorder. Eur J Pharm Sci. 2006;27(1):19–26.

18. Witzleb R, Kanikanti V-R, H-Jr H, Kleinebudde P. Influence of needle-shaped drug particles on the solid lipid extrusion process. Powder Technol. 2011;207(1–3):407–13.

19. Garekani HA, Sadeghi F, Badiee A, Mostafa SA, Rajabi-Siahboomi AR. Crystal habit modifications of ibuprofen and their physicomechanical characteristics. Drug Dev Ind Pharm. 2001;27(8):803–9.

20. Heng JYY, Bismarck A, Williams DR. Anisotropic surface chemistry of crystalline pharmaceutical solids. AAPS PharmSciTech. 2006;7(4):E12–20. Article 84.

21. Thielmann F, Burnett DJ, Heng JYY. Determination of the surface energy distributions of different processed lactose. Drug Dev Ind Pharm. 2007;33(11):1240–53.

22. Kaminsky W, Glazer AM. Crystal optics of D-mannitol, C6H14O6: Crystal growth, structure, basic physical properties, birefringence, optical activity, Faraday effect, electro-optic effects and model calculations. Zeitschrift fur Kristallographie. 1997;212(4):283–96.

23. Ho R, Hinder SJ, Watts JF, Dilworth SE, Williams DR, Heng JYY. Determination of surface heterogeneity of D-mannitol by sessile drop contact angle and finite concentration inverse gas chromatography. Int J Pharm. 2010;387(1–2):79–86.

24. Docherty R, Clydesdale G, Roberts KJ, Bennema P. Application of Bravais-Friedel-Donnay-Harker, attachment energy and Ising-models to predicting and understanding the morphology of molecular-crystals. J Phys D Appl Phys. 1991;24(2):89–99.

25. Sun CC, Kiang YH. On the identification of slip planes in organic crystals based on attachment energy calculation. J Pharm Sci. 2008;97(8):3456–61.

26. Grimsey IM, Sunkersett M, Osborn JC, York P, Rowe RC. Interpretation of the differences in the surface energetics of two optical forms of mannitol by inverse gas chromatography and molecular modelling. Int J Pharm. 1999;191(1):43–50.

27. Yu L, Mishra DS, Rigsbee DR. Determination of the glass properties of D-mannitol using sorbitol as an impurity. J Pharm Sci. 1998;87(6):774–7.

28. Yoshinari T, Forbes RT, York P, Kawashima Y. Crystallisation of amorphous mannitol is retarded using boric acid. Int J Pharm. 2003;258(1–2):109–20.

29. Willart JF, Descamps N, Caron V, Capet F, Danede F, Descamps M. Formation of lactose-mannitol molecular alloys by solid state vitrification. Solid State Comm. 2006;138(4):194–9.

30. Ghadiri M, Zhang Z. Impact attrition of particulate solids. Part 1: a theoretical model of chipping. Chem Eng Sci. 2002;57(17):3659–69.